

Optimizing Cervical Target Volume in Patients with Nasopharyngeal Cancer Based On Nodal Drainage Distance



Yang Liu¹, Wenbin Yan², Chaosu Hu², Xiaodong Huang¹, Kai Wang¹, Yuan Qu¹, Xuesong Chen¹, Runye Wu¹, Ye Zhang¹, Jianghu Zhang¹, Jingwei Luo¹, Yexiong Li¹, Jingbo Wang¹, and Junlin Yi^{1,3}

ABSTRACT

Purpose: To determine the potential nodal drainage distances of nasopharyngeal carcinoma (NPC) by investigating spatial distribution of metastatic lymph nodes (LN).

Experimental Design: Patients with NPC harboring at least two ipsilateral metastatic LNs were enrolled. LN spreading distances were analyzed in nonrestricted direction, cranial-to-caudal direction, and between the two most caudal LNs. Euclidean distance (ED) and vertical distance (VD) between any two LNs were computed. The nearest-neighbor ED and VD covering 95% of LNs or patients (p95-ED and p95-VD) were considered drainage distances, and were further validated by independent internal and external cohorts with recurrent LNs.

Results: In all, 5,836 metastatic LNs in 948 patients were contoured. Corresponding to the three scenarios, per-LN level, the p95-EDs were 2.83, 3.28, and 3.55 cm, and p95-VDs

were 2.17, 2.32, and 2.63 cm, respectively. Per-patient level, the p95-EDs were 3.25, 3.95, and 3.81 cm, and p95-VDs were 2.67, 2.81, and 2.73 cm, respectively. In internal validation, over 95% of recurred LNs occurred within ED of 2.91 cm and VD of 0.82 cm to the neighbor LN, and the corresponding distances in external validation were 2.77 and 0.67 cm, respectively.

Conclusions: In NPC, the maximum LN drainage distance was 3.95 cm without considering the direction. Specifically, in cranial-to-caudal direction, the sufficient vertical drainage distance was 2.81 cm, indicating that a 3-cm extension from the most inferior node may be rational as caudal border of the prophylactic clinical target volume (CTV). These findings promote in-depth understanding of nodal spreading patterns, uncovering paramount evidence for individualized CTV.

Introduction

Nasopharyngeal carcinoma (NPC) is one of the most common malignant tumors of the head and neck. Multidisciplinary treatment and advances in radiotherapy techniques have yielded markedly improved treatment outcomes in patients with NPC, with the 5-year overall survival rates now exceeding 80% (1–3). In the era of intensity-modulated radiotherapy, precise delineation of neck clinical target volume (CTV) is critical to ensure excellent locoregional control while avoiding severe adverse effects on organ function.

Cervical lymph node (LN) metastasis is common in NPC cases. Currently, contouring of cervical CTV for NPC is based on the extent of LN involvement and anatomical nodal regions. International guidelines recommend coverage of bilateral retropharyngeal LNs and levels II, III, and Va within CTV for all T and N categories, and coverage of

ipsilateral cervical LN levels IV and Vb for cases of ipsilateral involved cervical LNs (4). Because skip LN involvement is scarce and in-field recurrence is the main pattern of regional failure, deducing that the lymphatic spread of NPC may be a function of distance from the gross tumor, rather than rigidly following the anatomical landmarks, is reasonable (5–7).

In previous studies investigating cervical target of NPC, CTV delineation was primarily determined by the involved region and the distribution of preexisting metastatic LNs in a group of patients (8, 9). This mapping-based CTV remains a “one-fits-all” strategy, which is largely affected by the selection bias and does not allow individualized delineation at per-patient or per-nodal levels. Utilizing a meticulous method for nodal distribution, spatial analysis enables the distance computation between any two points, thereby obtaining the potential drainage distance between two LNs.

This study aimed to explore the spatial distribution of metastatic cervical LNs in a large cohort of patients with NPC to obtain an LN drainage pattern. The metastatic LN drainage distances were analyzed at both per-LN level and per-patient level to uncover paramount distance evidence for adjusting and individualizing cervical CTV delineation in NPC.

Materials and Methods

Training patient cohort

A total of 2,122 consecutive patients with pathologically proven NPC were treated in our center from January 2010 to December 2021. Among them, eligible patients were screened by utilizing the following criteria: (i) with at least two metastatic LNs on one side of the neck and (ii) who underwent simulation MRI scans of the nasopharynx and neck. Eventually, 948 patients were included in the final analysis. Supplementary Fig. S1 shows the patient selection process. This study

¹Department of Radiation Oncology, National Cancer Center/National Clinical Research Center for Cancer/Cancer Hospital, Chinese Academy of Medical Sciences and Peking Union Medical College, Beijing, China. ²Department of Radiation Oncology, Fudan University Shanghai Cancer Center, Shanghai, China. ³Department of Radiation Oncology, National Cancer Center/National Clinical Research Center for Cancer/Hebei Cancer Hospital, Chinese Academy of Medical Sciences (CAMS), Langfang, Hebei Province, China.

Corresponding Authors: Junlin Yi, Department of Radiation Oncology, Cancer Hospital of Chinese Academy of Medical Sciences, No. 17, Panjiayuan Nanli, Beijing, 100021, China. E-mail: yijunlin1969@163.com; and Jingbo Wang, wangjingbo201001@163.com

Clin Cancer Res 2024;30:1801–10

doi: 10.1158/1078-0432.CCR-23-23274

This open access article is distributed under the Creative Commons Attribution-NonCommercial-NoDerivatives 4.0 International (CC BY-NC-ND 4.0) license.

©2024 The Authors; Published by the American Association for Cancer Research

Translational Relevance

This study is the first to uncover the cervical lymph node (LN) drainage distance based on LN's spatial distribution in nasopharyngeal carcinoma (NPC). Unlike conventional mapping-based nodal distribution, spatial analysis can compute the distance between two given LNs using each node coordinate. The LN drainage distances were analyzed in three paradigms, comprising all potential drainage modalities of the cervical nodes.

On the basis of cervical LN drainage distances at per-patient and per-nodal levels, we further proposed a reduced clinical target volume (CTV), utilizing distances that could cover the drainage distances of 95% LNs and patients. Compared with anatomical landmarks or fixed distance-based CTV borders, our data could provide more precise and individualized evidence for CTV delineation in NPC. The rationality of this CTV delineation was further validated by independent internal and external cohorts with regional recurrent LNs.

This study provides deeper insights into nodal spreading patterns and uncovers important strategies for CTV optimization by adopting individual LN drainage distances instead of utilizing uniform anatomical landmarks.

was conducted in accordance with ethical guidelines as outlined by the Declaration of Helsinki. Ethical approval and a waiver of informed consent were obtained from the institutional review board (#23/353-4095).

Imaging acquisition and transfer

CT (Philips Brilliance) and MRI scans (GE Discovery; parameters: T1WI, TE: Min Full; frequency: 352; phase: 256; NEX, 2.00; slice thickness: 3 mm; spacing: 0.0; Freq. FOV, 28.0. T2WI, TE: 68.0; frequency: 320; phase: 224; NEX, 1.00; slice thickness: 3 mm; spacing: 0.0; Freq. FOV, 28.0.) were performed during preradiation simulation, with the patient in the supine position and with thermoplastic mask immobilization at the head, neck, and shoulder. Scans were captured in 3-mm slices from the top of the head to 2 cm below the sternoclavicular joint. The CT and MR images were transferred to MIM (version 7.1.4) system in DICOM format.

LN contouring and marking

Metastatic LN was identified according to international consensus (4). The diagnostic criteria for metastatic cervical LNs identification were outlined as follows: cervical LNs presenting the minimum axial diameter ≥ 10 mm; retropharyngeal nodes in the lateral group with the minimum axial diameter ≥ 5 mm in the largest plane; any visible node in the median group; LNs demonstrating central necrosis or a contrast-enhancing rim; nodal grouping characterized by ≥ 3 contiguous and confluent LNs, each with a minimum axial diameter of 8 to 10 mm; LNs of any size exhibiting extranodal extension (4, 10).

On each patient's simulation MR images, two radiation oncologists with at least 5 years of experience specializing in NPC reviewed all images of each patient and marked the LNs with malignant features. Each radiation oncologist identified and marked the LNs independently, masked to each other. Then, the contours were cross-checked and compared to generate the final ones for further analysis. Any disagreement was discussed face-to-face and referred to a third senior expert if needed until a final agreement was reached. The lateral process of the C1 (LPC1) was used as the reference landmark

because LPC1 is clearly visible and identifiable on MRI. Accordingly, the coordinates of the geometric centers of each contoured LN (X_{LN} , Y_{LN} , Z_{LN}) within each patient were automatically generated by the MIM system.

Internodal distance calculation based on spatial distribution

On the basis of each node coordinate, the three-dimensional distribution of all LNs within one side of the neck was visually constructed and available for further distance analysis. For patients with bilateral LN metastasis, the two sides of the neck were analyzed separately. **Figure 1A** displays schematic diagrams defining Euclidean distance (ED) and vertical distance (VD). The ED and VD between LNa (X_a , Y_a , Z_a) and any other LNx (X_x , Y_x , Z_x) were computed as follows:

$$\text{Euclidean distance (ED)} = \sqrt{(X_a - X_x)^2 + (Y_a - Y_x)^2 + (Z_a - Z_x)^2}$$

$$\text{Vertical distance (VD)} = |Z_a - Z_x|.$$

The schematic models for three scenarios of internodal distance calculation are shown in **Fig. 1B–D**. Internodal distance of LNs without considering the spread direction was first analyzed (**Fig. 1B**). Considering that LN metastasis is more likely to occur step by step in NPC with skip metastasis being very rare (5), we further assessed the cranial-to-caudal drainage distance. In this setting, the ED and VD distances between a given LN and all LNs located caudal to it were computed (**Fig. 1C**). Furthermore, we considered that the distance between the two LNs located most caudally from the primary lesion may represent the terminal extent of lymphatic drainage. Therefore, the ED and VD distances between the two most caudal LNs in each patient were evaluated (**Fig. 1D**).

Drainage distance derivation and analysis

Given that a metastatic LN is most likely to spread from the most adjacent LN, the nearest-neighbor Euclidean distance (nnED) and nearest-neighbor vertical distance (nnVD) were selected to represent the drainage distance of the given LN. All above-mentioned distance metrics were analyzed in two levels: per-LN level and per-patient level.

For the per-LN level, the 95th percentile of nnED (p95-ED) and nnVD (p95-VD) of all LNs from all patients were calculated to ensure coverage of at least 95% of the LN spreading distances. For per-patient level analysis, the p95-ED and p95-VD were first calculated for each patient, and the final 95th percentiles were subsequently obtained based on all p95-ED and p95-VD derived from each patient to ensure the coverage of LN extensions in at least 95% of the patients. For patients with bilateral cervical metastatic LNs, the larger one was selected for per-patient analysis.

Considering that nodal size may potentially impact metastatic LN drainage distances, the p95-ED and p95-VD were further investigated in each maximum diameter (MD) group at the per-LN level. At per-patient level, the influence of T stage and Epstein-Barr virus (EBV) DNA on LN drainage distances was also explored.

Internal and external validation cohorts with recurred LNs (Re-LN)

In the internal cohort, 141 of 2,122 patients suffered regional recurrence from January 2010 to December 2021. In the external cohort, 61 patients at the Fudan University Shanghai Cancer Center suffered regional recurrence from January 2017 to December 2020. Among them, 109 patients in the internal cohort and 60 patients in the external cohort with traceable radiotherapy plans and MRI images evidencing regional recurrence were selected as the internal and

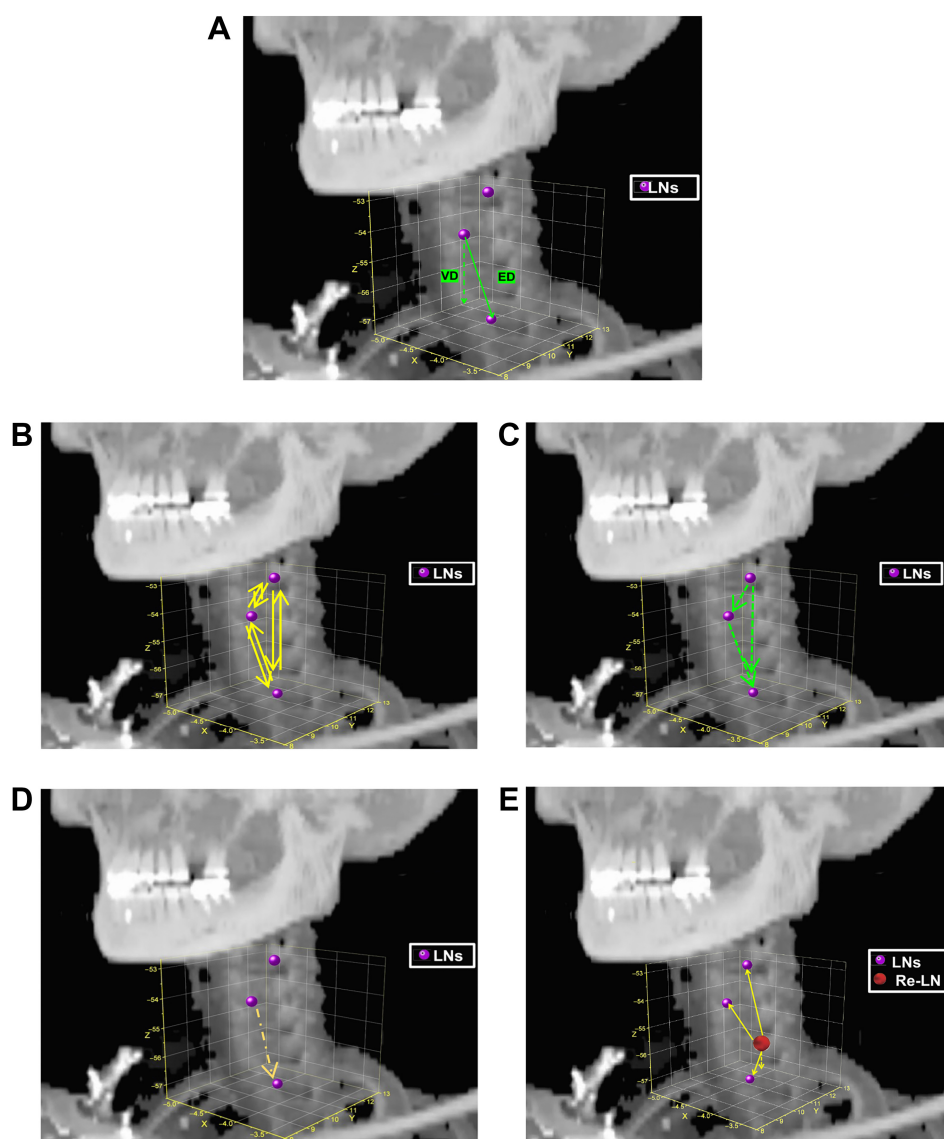


Figure 1.

A, Schematic diagrams defining ED and VD. $ED = \sqrt{(Xa - Xx)^2 + (Ya - Yx)^2 + (Za - Zx)^2}$; $VD = |Za - Zx|$. **B**, Distribution pattern of LNs without restricted metastatic direction: the nnED and nnVD were computed between any pair of center coordinates of all contoured LNs. **C**, Distribution pattern of LNs in cranial-to-caudal metastatic direction: the nnED and nnVD were computed between a given LN and all LNs located more caudal to it. **D**, Distribution pattern between the most caudal two metastatic LNs. **E**, Distribution pattern of Re-LNs: the nnED and nnVD were calculated between Re-LNs and the original neighbor metastatic LNs.

external validation cohorts. Notably, all recurrent LNs were confirmed by histology or at least two imaging studies.

The MRI images at initial diagnosis and at recurrence, as well as the original simulation images and radiotherapy plan, were all imported into the MIM system and were registered using the bony markers. The involved LNs prior to treatment and Re-LNs were both marked on the initial MR images referring to the surrounding anatomic details.

The ED and VD distances were calculated between the Re-LN and the ipsilateral original metastatic LNs (Fig. 1E). Similar to the training cohort, a recurrent LN was considered most likely to spread from the closest original LN (O-LN) in the validation cohort. Therefore, the nnED for Re-LN (nnED-R) and the nnVD for Re-LN (nnVD-R) were calculated to represent the recurrence ability of the O-LN.

Statistical analysis

Statistical analysis was performed using SPSS 22.0, Python 2022.2.1, and Origin 2019b. The cdist function in the Python packages SciPy (1.4.1) was rendered to compute the ED and VD distances between the centers of any two contoured LNs (11). Continuous variables were described using median (range) and evaluated utilizing nonparametric tests. Categorical variables were tested using the chi-square test. Statistical significance was considered at $P < 0.05$.

Data availability

The de-identified patient datasets for the training, internal and external validation cohorts, along with the raw data for analysis presented in tables and figures, have been uploaded and are accessible

at <https://zenodo.org/records/10608499>. An investigator who wishes to analyze data from this work must make a formal request to the corresponding author.

Results

Table 1 lists the patients' characteristics in the training, internal validation, and external validation cohorts. Of the 948 patients in the training cohort, 8.8% (83/948) had stage II tumors, 50.3% (477/948) had stage III tumors, and 40.9% (388/948) had stage IVA tumors. In terms of the LN distribution, 538 (56.8%) had unilateral and 410 (43.2%) had bilateral LN involvement, respectively. Therefore, a total of 1,358 sets ($410 \times 2 + 538 = 1,358$) of LNs (5,836 LNs in all) were marked. The median MD was 2.12 cm (range, 0.61–10.56 cm). Supplementary Fig. S2 shows the number and proportion of LNs in each MD group.

Figure 2A presents the overall distribution pattern of metastatic LNs. The median VD of the contoured LNs to LPC1 was 3.40 cm (range, 0–13.64 cm). **Figure 2B** demonstrates the number and percentage of caudal LN correspondence with each VD range from LPC1. **Figure 2C** shows 95% of the LNs located within 8.60 cm inferior to LPC1.

Table 1. Characteristics of training and validation cohorts.

Variable	Training cohort (n = 948)	Internal validation cohort (n = 109)	External validation cohort (n = 60)
Sex			
Male	637 (67.2)	78 (71.6)	41 (68.3)
Female	311 (32.8)	31 (28.4)	19 (31.7)
Age, years			
Median (range)	48 (18–83)	47 (21–77)	47 (19–78)
<50	335 (35.3)	42 (38.5)	18 (30.0)
≥50	613 (64.7)	67 (61.5)	42 (70.0)
Histologic type			
Keratinizing	4 (0.4)	2 (1.8)	1 (1.7)
Nonkeratinizing	944 (99.6)	107 (98.2)	59 (98.3)
8th AJCC T stage			
T1	114 (12.0)	19 (17.4)	7 (11.7)
T2	140 (14.8)	22 (20.2)	10 (16.7)
T3	390 (41.1)	45 (41.3)	30 (50.0)
T4	304 (32.1)	23 (21.1)	13 (21.6)
8th AJCC N stage			
N1	277 (29.2)	21 (19.3)	13 (21.7)
N2	553 (58.3)	52 (47.7)	26 (43.3)
N3	118 (12.4)	36 (33.0)	21 (35.0)
8th AJCC clinical stage			
II	83 (8.8)	6 (5.5)	2 (3.3)
III	477 (50.3)	53 (48.6)	33 (55.0)
IV	388 (40.9)	50 (45.9)	25 (41.7)
Lateral level of metastatic LN			
Unilateral	538 (56.8)	37 (33.9)	21 (35.0)
Bilateral	410 (43.2)	72 (66.1)	39 (65.0)
MD of LNs			
Median (range)	2.12 (0.61–10.56)	2.15 (0.78–10.51)	2.30 (0.80–9.81)
Pretreatment EBV DNA, copies/mL			
<500	416 (43.9)	40 (36.7)	20 (33.3)
500–2,000	449 (47.4)	59 (54.1)	29 (48.3)
>2,000	83 (8.7)	10 (9.2)	11 (18.4)

Abbreviations: N, node; T, tumor.

Supplementary Table S1 summarizes all ED and VD data in the three scenarios. For internodal distances without considering the spread direction, at the per-LN level, the p95-ED and p95-VD were 2.83 and 2.17 cm, respectively (**Fig. 3A**). At the per-patient level, the p95-ED and p95-VD to ensure adequate coverage of 95% of patients were 3.25 and 2.67 cm, respectively (**Fig. 3B**). The p95-ED and p95-VD tended to increase with increasing MD of LNs (**Fig. 4A and B**).

Supplementary Table S1 presents detailed ED and VD data for internodal distances in the cranial-to-caudal direction. At the per-LN level, the p95-ED and p95-VD were 3.28 and 2.32 cm, respectively (**Fig. 3C**). At the per-patient level, the p95-ED and p95-VD in the cranial-to-caudal direction to ensure coverage of 95% patients were 3.95 and 2.81 cm, respectively (**Fig. 3D**). The values of the p95-ED and p95-VD seemed to slightly increase with the MD of LNs (**Fig. 4C and D**).

Furthermore, employing the commonly used cutoff values for EBV DNA, 500 and 2,000 copies/mL, we divided the patients into three subgroups, <500, 500 to 2,000, and >2,000. All three groups exhibited similar patterns in the drainage distance in nonrestricted (Supplementary Figs. S3A and S3B) and cranial-to-caudal directions (Supplementary Figs. S3C and S3D). Besides EBV DNA, we investigated the impact of T stage on nodal drainage distance. Similarly, minimal differences were observed across all T1 to T4 subgroups, regardless of the potential spreading direction (Supplementary Figs. S4A–S4D).

Supplementary Table S1 also provides detailed ED and VD data for internodal distances between the most caudal two LNs. At the per-LN level, the p95-ED and VD distances of the most caudal two LNs were 3.55 and 2.63 cm, respectively (**Fig. 3E**). At the per-patient level, the p95-ED and p95-VD distances covering 95% of patients were 3.81 cm and 2.73 cm, respectively (**Fig. 3F**).

In the internal validation cohort of 109 patients with regional failure, 144 Re-LNs (median, 1; range, 1–6) and 873 O-LNs (median, 7; range, 1–47) were marked on the pretreatment MR images. The nnED-R and nnVD-R which covered 95% of patients were 2.91 and 0.82 cm (**Fig. 5A**), respectively, with both remarkably less than the corresponding distances in the initial three scenarios. The nnVD-R of 1, 2, and 3 cm from the nearest-neighbor O-LN covered 97.2%, 99.3%, and 100% of recurrent LNs, respectively (**Fig. 5B**).

In the external validation cohort of 60 patients with regional failure, 78 Re-LNs [median (range), 1 (1–4)] and 471 O-LNs [median (range), 5 (1–25)] were marked on the pretreatment MR images. The nnED-R and nnVD-R covering 95% of patients were 2.77 and 0.67 cm, respectively (**Fig. 5C**). These distances were numerically smaller than the corresponding ones in the internal validation cohort. The nnVD-R of 1 and 2 cm from the nearest-neighbor O-LN covered 94.9% and 100% of recurrent LNs (**Fig. 5D**).

Notably, VDs of Re-LN from LPC1 [median (range), 3.0 (1.2–10.8) cm for the internal validation cohort and 4.1 (2.0–9.2) cm for the external validation cohort] were all shorter than that of the lowest initial ipsilateral LN to LPC1 [median (range), 5.6 (0.5–11.2) cm for the internal validation cohort and 6.3 (1.1–10.3) cm for the external validation cohort; both $P < 0.001$], indicating no LN relapsing out of the inferior border of initial nodal gross tumor volume (GTV). Furthermore, 131 (91.0%, 131/144) Re-LNs in the internal validation cohort, and 74 (94.9%, 74/78) in the external validation cohort were revealed to obtain the nnED and nnVD corresponding to the O-LN with the largest MD, indicating the high likelihood of a recurrent LN arising from the O-LN with the greatest nodal burden.

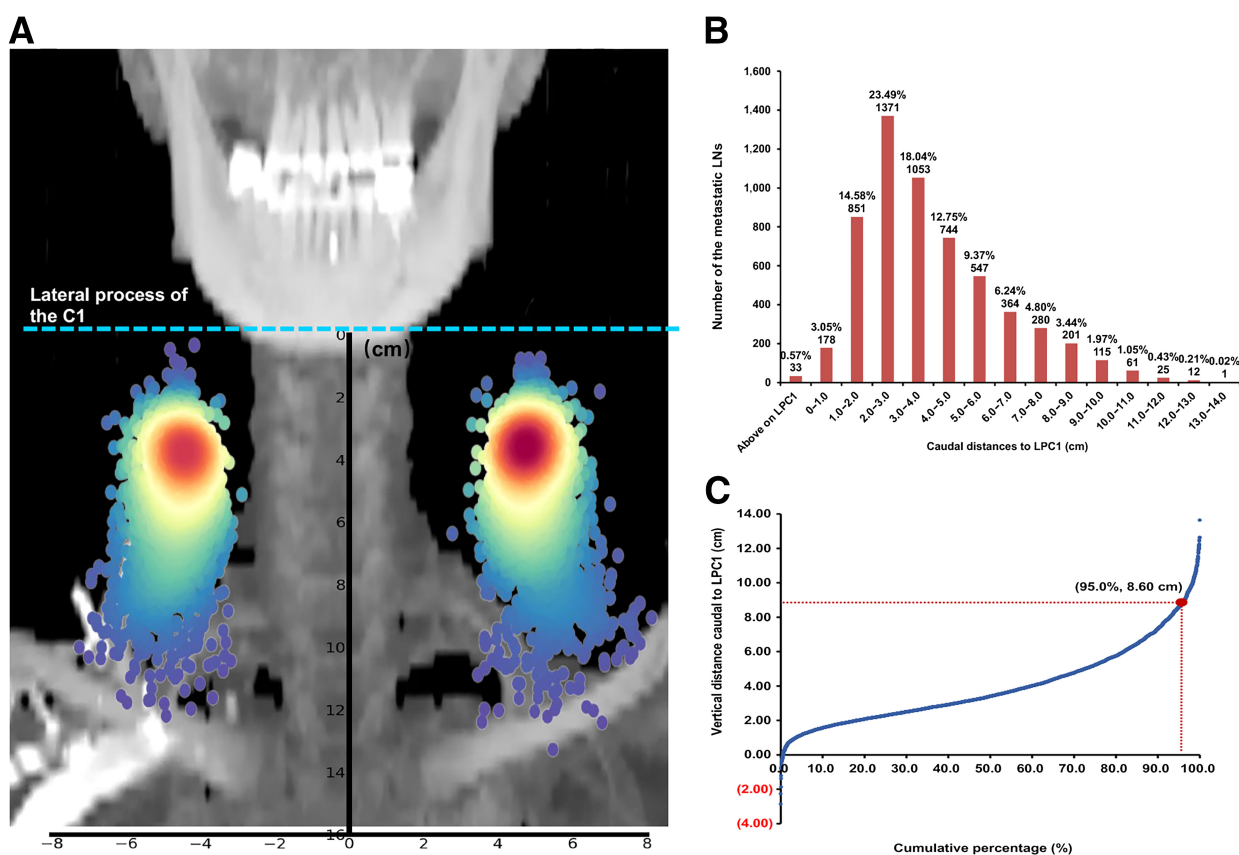


Figure 2. **A**, Probability heat map showing distribution of metastatic LNs using LPC1 as the reference. **B**, The number and percentage of the LNs included in each VD range below LPC1. **C**, The cumulative percentage curve of VD below LPC1 showing the distance at which 95% nodes were covered.

On the basis of the above distance data, we proposed a 3-cm expansion of the metastatic LN in the cranial-to-caudal direction as the inferior border of the cervical CTV. A selected patient with regional recurrence (175 cm, 70 kg man with T2N2M0 stage) is shown as an example (Fig. 5E and F). Two sets of the nodal CTV were delineated respectively as per the 2017 international guideline (CTV-consensus, Fig. 5E) and that proposed by the current study by extending 3 cm below the most caudal metastatic LNs (CTV-proposed, Fig. 5F). Correspondingly, the Re-LN was also marked on the same setting of MR according to anatomical location. Although the CTV-proposed was significantly reduced in the cranial-to-caudal direction compared with the CTV-consensus, it sufficiently covered the Re-LN (Fig. 5F).

Discussion

In this study, we investigated the LN drainage distances using spatial distribution analysis in a large cohort of patients with NPC. Our results revealed that a maximum Euclidean distance of 3.95 cm could reliably ensure coverage of LN drainage in any direction. Regarding the specific cranial-to-caudal direction, a maximum vertical distance of 2.81 cm was sufficient to safely cover the potential drainage route of the metastatic LN. These distances were further validated through analysis based on independent internal and external cohorts with regional recurrent LNs.

Currently, uniform borders across the different N categories are recommended for cervical CTV delineation in NPC (4, 12). Even the most recent effort at reducing the elective nodal irradiation volume still predominantly focused on avoiding irradiation to certain anatomical nodal regions, such as level IV (13–18). However, the actual lymphatic drainage should not have been restricted by the anatomical bony landmarks, as this is not in accordance with biological behavior. This method also does not consider individual anatomical variations. As a result, over 90% of patients suffer complications, such as hypothyroidism and subcutaneous fibrosis, which ultimately affect quality of life (19–22). Therefore, further optimization and individualization of cervical CTV is essential, especially for the caudal borders of the irradiation volume.

To determine LN distribution-based CTV design in NPC, the most commonly used approach is to mark all LNs from a group of patients on the template CT (8, 9, 23) and then obtain the CTV boundary by analyzing the LN distribution to generate a certain distance from the predefined hallmark (24). Nevertheless, this “one-size-fits-all” approach still does not allow individualized cervical target volume delineation as per the actual nodal status in each patient. By using the vertebrae as landmarks, a recent study showed the metastasis of cervical nodes at certain vertebral levels markedly correlated with two adjacent vertebral levels, including one level above and one below (25). Therefore, the author recommended that the low-risk CTV boarder could be reduced to two vertebral levels below that of

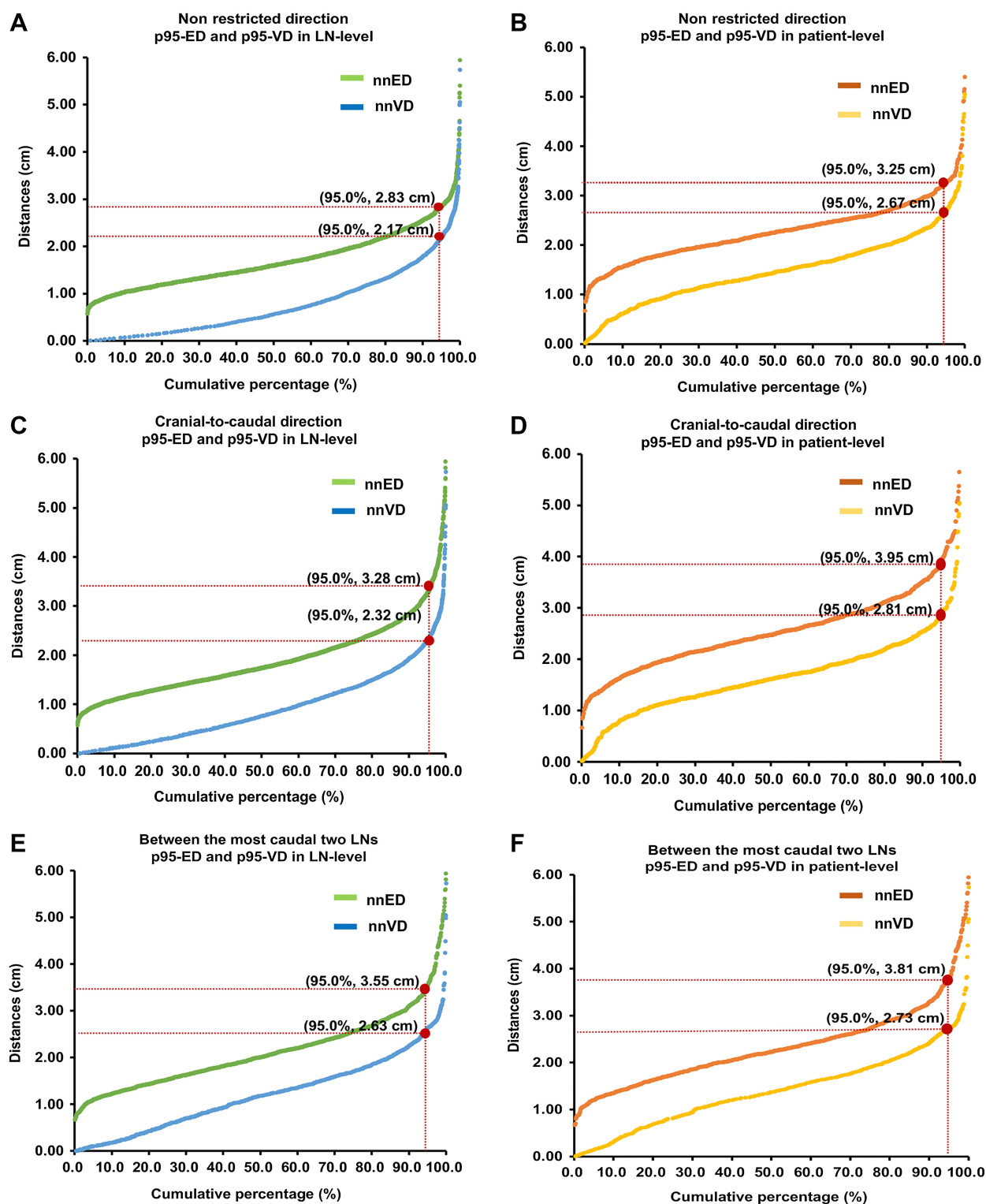


Figure 3.

Cumulative percentage of the distance coverage at per-nodal and per-patient levels for three direction scenarios. **A**, nnED and nnVD at the per-nodal level without considering direction. **B**, nnED and nnVD at the per-patient level without considering direction. **C**, nnED and nnVD at the per-nodal level in the cranial-to-caudal direction. **D**, nnED and nnVD at the per-patient level in the cranial-to-caudal direction. **E**, nnED and nnVD at the per-nodal level between the most caudal two LNs. **F**, nnED and nnVD at the per-patient level between the most caudal two LNs.

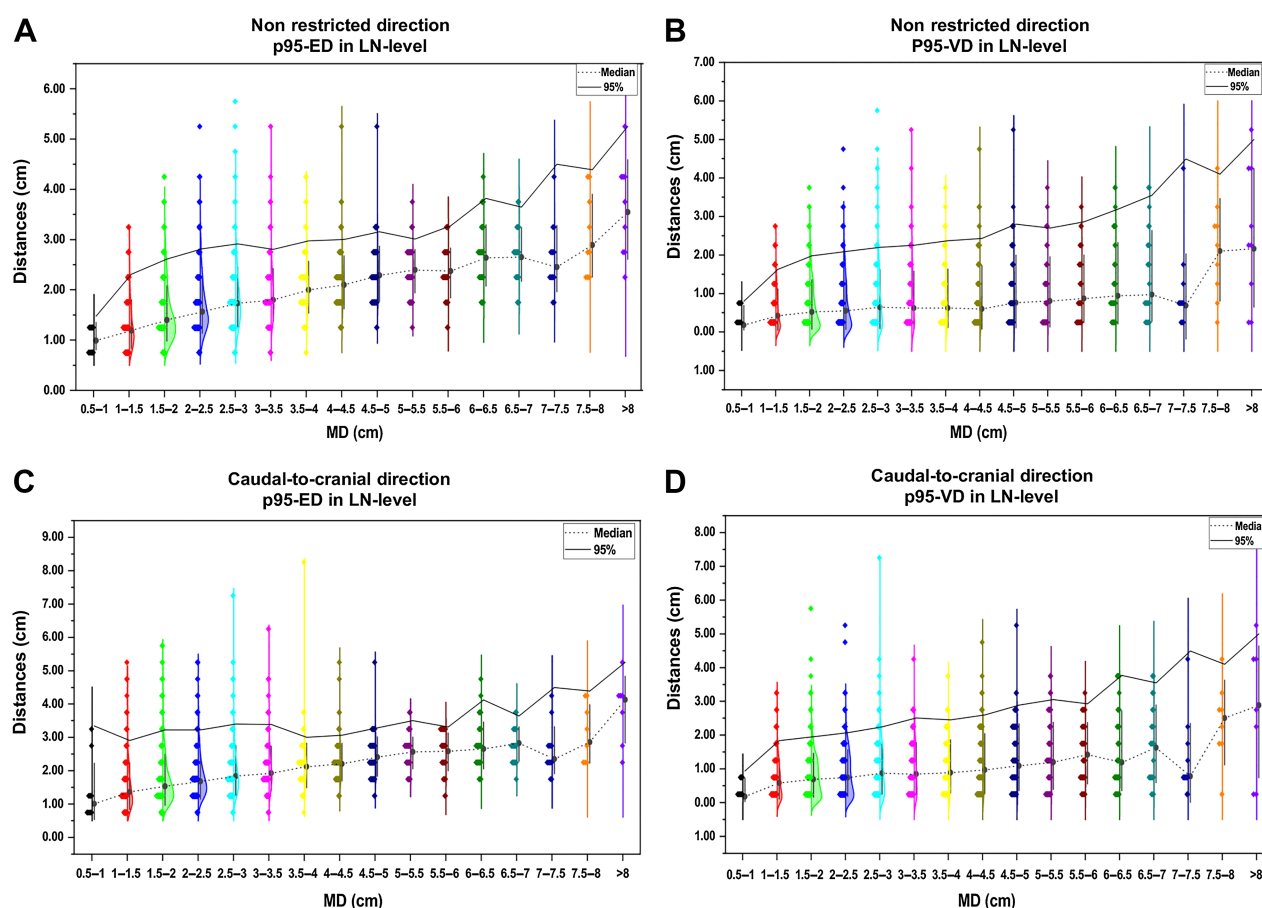


Figure 4.

Half-violin plots describing LN drainage distances in various MD groups. **A**, nnED without considering direction. **B**, nnVD without considering direction. **C**, nnED in the cranial-to-caudal direction. **D**, nnVD in the cranial-to-caudal direction.

metastatic nodes. Nevertheless, the vertebral level-based CTV border still varied according to the thickness and curvature of the cervical vertebral bodies. The distances between LNs could better quantify their spread ability and reflect the probable draining extent of LN metastases. This approach may provide more precise and individualized evidence for identifying prophylactic cervical irradiation in NPC.

To the best of our knowledge, this study is the first to perform cervical LN distribution-derived drainage distance analysis in NPC. We found that the 95% superior margin of distances between two neighbored LNs were 2.83, 3.28, and 3.55 cm, respectively, corresponding to the above-mentioned three scenarios. As expected, the distances tended to increase as MD increased. In per-patient level analysis, we considered all internodal measurements within each patient and ultimately selected the 95% upper bound as the representative distance for that patient. Analysis on the per-patient level revealed slightly larger distances according to the above scenarios while all remained below 4 cm. This approach minimized the underestimation of the drainage distance caused by the attenuation effect from other patients with closer internodal distances.

Interestingly, minimal differences in spreading distances were observed among patients in different EBV DNA strata and those with different T stages, in terms of LN distribution patterns without considering the spread direction and cranial-to-caudal direction. These findings imply that the LN spreading potentiality in NPC may

be independent of the overall tumor burden but more subject to the characteristics of the LN per se, such as nodal size. Accordingly, LN's contribution to high EBV DNA abundance is more attributed to the nodal burden, such as nodal size, volume, and number, than to each LN drainage ability. These observations may partly explain the special existence of the ascending type (advanced T stage whereas early N stage) and descending type (early T stage whereas advanced N stage) of NPC.

Because the caudal border is the most indecisive issue of the cervical irradiation volume in NPC, we specifically analyzed the spreading distance in the cranial-to-caudal direction. On the basis of the premise that spread along the neck lymphatic pathways is mostly in a cranial-to-caudal direction in NPC, with skip metastasis being very rare (26–28), we assumed that a given LN is most likely to receive drainage from its nearest cranial LN. We found that the internodal vertical distances with respect to the three distribution patterns were consistently less than 3 cm, indicating that 3-cm caudal irradiation to the metastatic LNs may be adequate to cover potential lymphatic spread. Therefore, we propose a 3-cm extension from the most inferior node as the caudal border of the prophylactic CTV (50–60 Gy equivalent). This proposal shared a similar tendency with the above-mentioned two vertebral-based expansions as the caudal border of the low-risk CTV (25). Moreover, our study provided distance data, offering a biologically rational basis for guiding elective radiation of

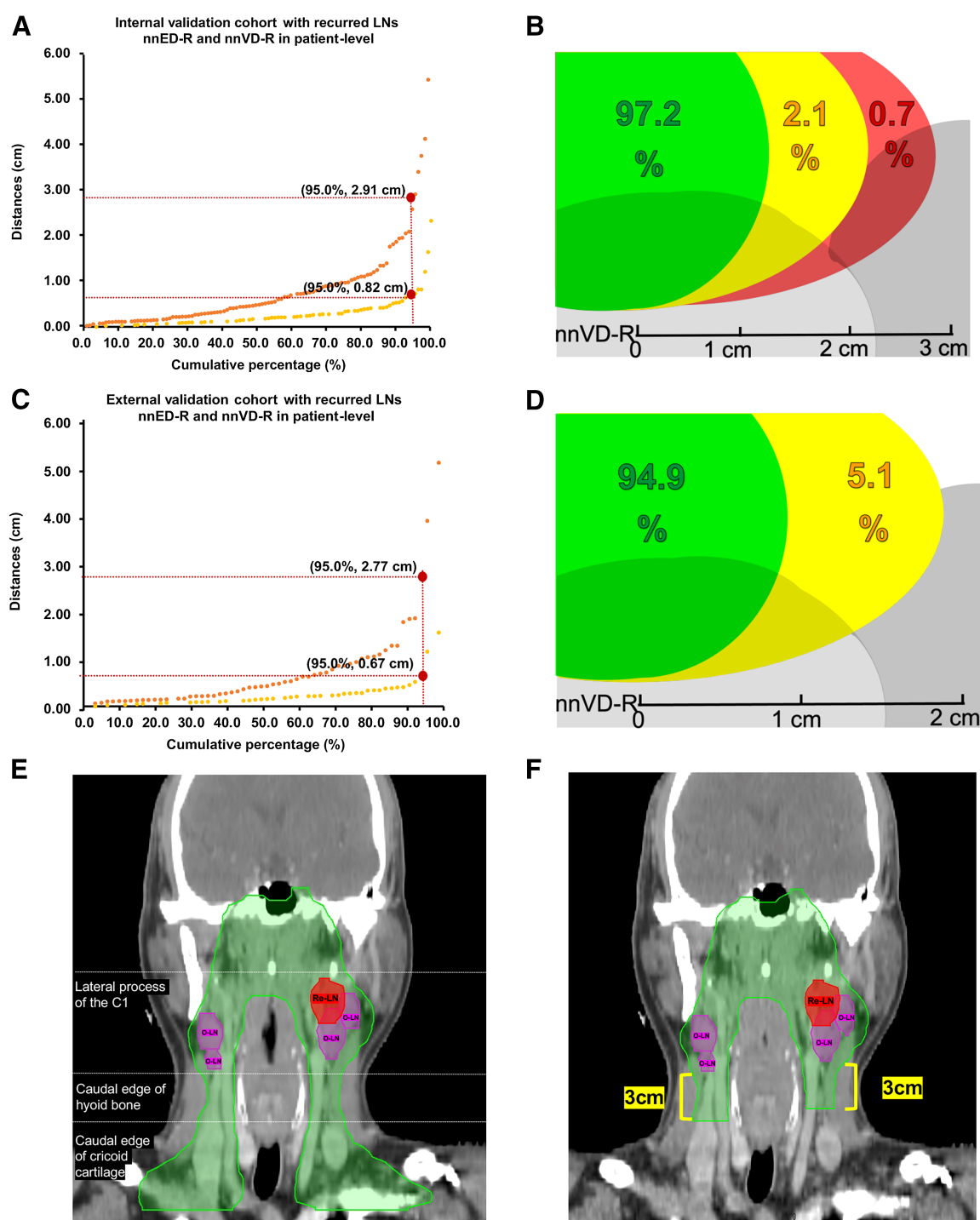


Figure 5.

A, Cumulative percentage curves showing nnED-R and nnVDs for Re-LNs (nnVD-R) covering 95% of patients in the internal validation cohort. **B**, The percentage of 1, 2, and 3 cm covering the nnVD-R between Re-LN and nearest-neighbor O-LN in the internal validation cohort. **C**, Cumulative percentage curves showing nnED-R and nnVD-R covering 95% of patients in the external validation cohort. **D**, The percentage of 1 and 2 cm covering the nnVD-R between Re-LN and nearest-neighbor O-LN in the external validation cohort. **E**, The nodal CTV delineated as per the 2017 international guideline and **(F)** 3 cm below the most caudal metastatic LNs as proposed by this study.

nodal regions. In support, a retrospective study reported regional control and the pattern of failure following selective neck irradiation with a lower elective radiation therapy dose in patients with NPC (16). By delivering only 36 Gy to the CTV at low risk that included a 2 to 2.5 cm distal margin from CTV at high risk (60 Gy) without considering the nodal level, authors of this study demonstrated a noninferior regional control rate (92.6% at 3 years and 91.4% at 5 years), as compared with the historical data from classical elective nodal irradiation policy. To some extent, these data provide additional evidence to support the rationality of the distance-based CTV reduction in NPC.

To validate this drainage distance-based CTV delineation, we selected patients who suffered regional recurrence to represent an overlook of the failure pattern. Marking the recurrent and O-LNs on the pretreatment simulation MR showed that the nnED and nnVD of the Re-LNs were 2.91 and 0.82 cm in the internal validation cohort and the corresponding distances were 2.77 and 0.67 cm in the external validation cohort, respectively. These distances were much smaller than the respective distances in the pretreatment setting. In addition, we observed no recurrent LN located more than 3 cm inferior to the original neighbor LN or inferior to the original caudal LN. Over 90% of the recurrent LNs were actually adjacent to the O-LN with the largest diameter. These data corroborated well with previous findings that the most regional recurrences are observed within the nodal GTV or CTVn1 region with high doses (70 Gy/60 Gy) and the marginal or out-of-field failure rates were below 10% (6, 7). This indicates that nodal failure in NPC may be more attributable to the local burden and intrinsic resistance to radiotherapy than to insufficient radiation volume, even with much lower radiotherapy doses. The validation data reinforced the reliability of the drainage distance-based cervical CTV delineation as well as the safety of nodal CTV reduction by using the 3-cm expansion below the gross nodal disease as the inferior border.

This study has several limitations. First, as a retrospective cohort study, the results are inevitably affected by selection biases to some extent. Second, the premise of our study hypothesis is that LNs metastasize consecutively with rare skip metastasis. Thus, our findings are inapplicable to cases with a potentially increased risk of skip metastasis, such as postoperative radiotherapy in patients receiving cervical nodal dissection or biopsy. Third, not all patients underwent PET/CT in this study. In this retrospective study, we enrolled patients receiving treatment between 2010 and 2021, during which the use of PET/CT increased gradually but was not mandatory. Favorably, all

radiotherapy plans were retrieved as a reference to identify nodal metastasis, which was especially helpful for ill-defined LNs on MR.

In conclusion, by investigating the spatial distribution of metastatic cervical LNs in this large population- and LN-based study, we found that the Euclidean and vertical distances of 3.95 and 2.81 cm could reliably cover the extent of nodal drainage in NPC. On the basis of the vertical distance data, we proposed that a 3-cm expansion of the metastatic LN in the cranial-to-caudal direction may be rational as the inferior border of the cervical CTV. These findings provide paramount evidence for optimizing the cervical CTV design by adopting the expansion distances of metastatic LNs instead of uniformly utilizing anatomical landmarks. Prospective validation is justified to verify the clinical utility of these distances and their validity in guiding cervical CTV delineation.

Authors' Disclosures

No disclosures were reported.

Authors' Contributions

Y. Liu: Data curation, formal analysis, supervision, investigation, writing—original draft, writing—review and editing. **W. Yan:** Investigation, writing—review and editing. **C. Hu:** Investigation, writing—review and editing. **X. Huang:** Investigation, writing—review and editing. **K. Wang:** Investigation, writing—review and editing. **Y. Qu:** Investigation, writing—review and editing. **X. Chen:** Investigation, writing—review and editing. **R. Wu:** Investigation, writing—review and editing. **Y. Zhang:** Investigation, writing—review and editing. **J. Zhang:** Investigation, writing—review and editing. **J. Luo:** Investigation, writing—review and editing. **Y. Li:** Investigation, writing—review and editing. **J. Wang:** Data curation, formal analysis, supervision, funding acquisition, investigation, methodology, writing—original draft, writing—review and editing. **J. Yi:** Data curation, formal analysis, investigation, funding acquisition, writing—original draft, writing—review and editing.

Acknowledgments

This work was supported by the National High Level Hospital Clinical Research Funding (2022-CICAMS-80102022203) to J. Yi; Chinese Academy of Medical Sciences (CAMS) Innovation Fund for Medical Sciences (grant nos. 2021-I2M-C&T-B-070 and 2021-I2M-C&T-A-018) to J. Wang and R. Wu; and the Beijing hope run fund (grant nos. LC2021L06 and LC2022A26) to J. Yi and J. Wang.

Note

Supplementary data for this article are available at Clinical Cancer Research Online (<http://clincancerres.aacrjournals.org/>).

Received October 24, 2023; revised December 21, 2023; accepted February 9, 2024; published first February 13, 2024.

References

- Blanchard P, Lee A, Marguet S, Leclercq J, Ng WT, Ma J, et al. Chemotherapy and radiotherapy in nasopharyngeal carcinoma: an update of the MAC-NPC meta-analysis. *Lancet Oncol* 2015;16:645–55.
- Sun X, Su S, Chen C, Han F, Zhao C, Xiao W, et al. Long-term outcomes of intensity-modulated radiotherapy for 868 patients with nasopharyngeal carcinoma: an analysis of survival and treatment toxicities. *Radiother Oncol* 2014;110:398–403.
- Tian YM, Liu MZ, Zeng L, Bai L, Lin CG, Huang SM, et al. Long-term outcome and pattern of failure for patients with nasopharyngeal carcinoma treated with intensity-modulated radiotherapy. *Head Neck* 2019;41:1246–52.
- Lee AW, Ng WT, Pan JJ, Poh SS, Ahn YC, AlHussain H, et al. International guideline for the delineation of the clinical target volumes (CTV) for nasopharyngeal carcinoma. *Radiother Oncol* 2018;126:25–36.
- Wang X, Hu C, Ying H, He X, Zhu G, Kong L, et al. Patterns of lymph node metastasis from nasopharyngeal carcinoma based on the 2013 updated consensus guidelines for neck node levels. *Radiother Oncol* 2015;115:41–5.
- Xue F, Hu C, He X. Long-term patterns of regional failure for nasopharyngeal carcinoma following intensity-modulated radiation therapy. *J Cancer* 2017;8:993–9.
- Li S, Wang K, Hou Z, Yang J, Ren W, Gao S, et al. Use of radiomics combined with machine learning method in the recurrence patterns after intensity-modulated radiotherapy for nasopharyngeal carcinoma: a preliminary study. *Front Oncol* 2018;8:648.
- Lin L, Lu Y, Wang XJ, Chen H, Yu S, Tian J, et al. Delineation of neck clinical target volume specific to nasopharyngeal carcinoma based on lymph node distribution and the international consensus guidelines. *Int J Radiat Oncol Biol Phys* 2018;100:891–902.
- Jing H, Wang SL, Li J, Xue M, Xiong ZK, Jin J, et al. Mapping patterns of ipsilateral supraclavicular nodal metastases in breast cancer: rethinking the clinical target volume for high-risk patients. *Int J Radiat Oncol Biol Phys* 2015;93:268–76.
- van den Brekel MW, Stel HV, Castelijns JA, et al. Cervical lymph node metastasis: assessment of radiologic criteria. *Radiology* 1990;177:379–84.

11. Virtanen P, Gommers R, Oliphant TE, Haberland M, Reddy T, Cournapeau D, et al. SciPy 1.0: fundamental algorithms for scientific computing in Python. *Nat Methods* 2020;17:261–72.
12. Gregoire V, Levendag P, Ang KK, Bernier J, Braaksma M, Budach V, et al. CT-based delineation of lymph node levels and related CTVs in the node-negative neck: DAHANCA, EORTC, GORTEC, NCIC, RTOG consensus guidelines. *Radiother Oncol* 2003;69:227–36.
13. Wijers OB, Levendag PC, Tan T, van Dieren EB, van Sörnsen de Koste J, van der Est H, et al. A simplified CT-based definition of the lymph node levels in the node negative neck. *Radiother Oncol* 1999;52:35–42.
14. Gao Y, Zhu G, Lu J, Ying H, Kong L, Wu Y, et al. Is elective irradiation to the lower neck necessary for N0 nasopharyngeal carcinoma? *Int J Radiat Oncol Biol Phys* 2010;77:1397–402.
15. Chen JZ, Le QT, Han F, Lu LX, Huang SM, Lin CG, et al. Results of a phase 2 study examining the effects of omitting elective neck irradiation to nodal levels IV and Vb in patients with N(0–1) nasopharyngeal carcinoma. *Int J Radiat Oncol Biol Phys* 2013;85:929–34.
16. Cho WK, Oh D, Lee E, Kim TG, Lee H, Nam H, et al. Feasibility of selective neck irradiation with lower elective radiation dose in treating nasopharynx cancer patients. *Cancer Res Treat* 2019;51:603–10.
17. Huang CL, Xu C, Zhang Y, Zhou GQ, Mao YP, Liu Q, et al. Feasibility of ipsilateral lower neck sparing irradiation for unilateral or bilateral neck node-negative nasopharyngeal carcinoma: systemic review and meta-analysis of 2,521 patients. *Radiat Oncol* 2018;13:141.
18. Tang LL, Huang CL, Zhang N, Jiang W, Wu YS, Huang SH, et al. Elective upper-neck versus whole-neck irradiation of the uninvolved neck in patients with nasopharyngeal carcinoma: an open-label, non-inferiority, multicentre, randomised phase 3 trial. *Lancet Oncol* 2022;23:479–90.
19. McDowell LJ, Rock K, Xu W, Chan B, Waldron J, Lu L, et al. Long-term late toxicity, quality of life, and emotional distress in patients with nasopharyngeal carcinoma treated with intensity modulated radiation therapy. *Int J Radiat Oncol Biol Phys* 2018;102:340–52.
20. Lin YH, Huang TL, Chien CY, Chen HC, Hsu HC, Huang EY, et al. Pretreatment prognostic factors of survival and late toxicities for patients with nasopharyngeal carcinoma treated by simultaneous integrated boost intensity-modulated radiotherapy. *Radiat Oncol* 2018;13:45.
21. Zheng Y, Han F, Xiao W, Xiang Y, Lu L, Deng X, et al. Analysis of late toxicity in nasopharyngeal carcinoma patients treated with intensity modulated radiation therapy. *Radiat Oncol* 2015;10:17.
22. Zhao C, Miao JJ, Hua YJ, Wang L, Han F, Lu LX, et al. Locoregional control and mild late toxicity after reducing target volumes and radiation doses in patients with locoregionally advanced nasopharyngeal carcinoma treated with induction chemotherapy (IC) followed by concurrent chemoradiotherapy: 10-year results of a phase 2 study. *Int J Radiat Oncol Biol Phys* 2019;104:836–44.
23. Nijkamp J, Kusters M, Beets-Tan RG, Martijn H, Beets GL, van de Velde CJ, et al. Three-dimensional analysis of recurrence patterns in rectal cancer: the cranial border in hypofractionated preoperative radiotherapy can be lowered. *Int J Radiat Oncol Biol Phys* 2011;80:103–10.
24. Zhao Y, Liao X, Wang Y, Lan W, Ren J, Yang N, et al. Level Ib CTV delineation in nasopharyngeal carcinoma based on lymph node distribution and topographic anatomy. *Radiother Oncol* 2022;172:10–7.
25. Zhu GL, Zhang XM, Yang KB, Tang LL, Ma J. Metastatic patterns of level II-V cervical lymph nodes assessed per vertebral levels in nasopharyngeal carcinoma. *Radiother Oncol* 2023;179:109447.
26. Ho FC, Tham IW, Earnest A, Lee KM, Lu JJ. Patterns of regional lymph node metastasis of nasopharyngeal carcinoma: a meta-analysis of clinical evidence. *BMC Cancer* 2012;12:98.
27. Sham JS, Choy D, Wei WI. Nasopharyngeal carcinoma: orderly neck node spread. *Int J Radiat Oncol Biol Phys* 1990;19:929–33.
28. Tang L, Mao Y, Liu L, Liang S, Chen Y, Sun Y, et al. The volume to be irradiated during selective neck irradiation in nasopharyngeal carcinoma: analysis of the spread patterns in lymph nodes by magnetic resonance imaging. *Cancer* 2009;115:680–8.